Reac Kinet Mech Cat (2015) 116:371–383
DOI 10.1007/s11144-015-0906-4

Synthesis and 1-butene hydrogenation activity of platinum decorated bamboo-shaped multiwall carbon nanotubes

László Vanyorek[1] · Ferenc Kristály[2] · Andrea Mihalkó[3] · Olivér Bánhidi[1] · Ákos Kukovecz[4,5] · Zoltán Kónya[4,6] · János Lakatos[1]

Received: 20 May 2015 / Accepted: 21 July 2015 / Published online: 28 July 2015

Abstract Bamboo-shaped carbon nanotubes (BCNT) were prepared from three different amines on supported iron (Fe) and nickel (Ni) catalysts by catalytic chemical vapor deposition. The main factors governing product morphology and defect site density were identified. Post-synthetic oxidative functionalization was used to add carboxyl groups to the nanotubes, and then platinum (Pt) nanoparticles were deposited on the surface by the in situ reduction of a platinum salt. The average Pt nanoparticle diameter was found to be affected by the extent of surface functionalization. The catalytic performance of the synthesized Pt/BCNT samples were examined in the hydrogenation of 1-butene, in order to show that the catalytic activity of the bamboo like carbon nanotube supported Pt catalyst is similar to the conventional Pt catalysts in heterogeneous catalytic hydrogenation. The best overall performance was achieved when the bamboo-shaped nanotube support was

Electronic supplementary material The online version of this article (doi:10.1007/s11144-015-0906-4) contains supplementary material, which is available to authorized users.

✉ László Vanyorek
kemvanyi@uni-miskolc.hu

[1] Institute of Chemistry, University of Miskolc, Miskolc-Egyetemváros 3515, Hungary

[2] Institute of Mineralogy and Geology, University of Miskolc, Miskolc-Egyetemváros 3515, Hungary

[3] Wanhua BorsodChem Zrt, Bolyaitér 1, Kazincbarcika 3700, Hungary

[4] Department of Applied & Environmental Chemistry, University of Szeged, Rerrich B. tér 1, Szeged 6720, Hungary

[5] MTA-SZTE "Lendület" Porous Nanocomposites Research Group, Rerrich B. tér 1, Szeged 6720, Hungary

[6] MTA-SZTE Reaction Kinetics and Surface Chemistry Research Group, Rerrich B. tér 1, Szeged 6720, Hungary

synthesized on 5 wt% Fe/Al(OH)$_3$ catalyst from triethylamine and decorated with 5 wt% platinum nanoparticles.

Keywords Bamboo-shaped multiwall carbon nanotubes · Catalyst support · 1-Butene hydrogenation

Introduction

Carbon nanotubes (CNTs) are promising heterogeneous catalyst support materials because of their high specific surface area, good mechanical/thermal stability and anisotropic structure. Recent successes in CNT-based heterogeneous catalysis include hydrodesulfurization [1], hydroformylation [2], Fischer–Tropsch [3], oxidation [4] and hydrogenation reactions [5]. Tailoring the morphology of nanocarbons has been shown to be effective in fine-tuning the performance of catalysts. Their special interaction with deposited metals makes carbon nanotubes good heterogeneous catalytic support materials [6–8]. When the performance of catalysts supported on nanotubes and other carbon allotropes was compared in e.g. the dehydrogenation of ethyl-benzene and the hydrogenation of nitro-cyclohexane and methyl-styrene, higher catalytic activity and selectivity was observed over CNT-supported catalysts [9–11]. In the dehydrogenation of 1-butene the formation rate of butadiene was more than 10 times higher on CNTt han that of activated carbon. [12].

Bamboo-shaped carbon nanotubes (BCNTs) are a special type of multiwall carbon nanotubes, characterized by an inner channel that is sectioned by half-fullerene spheres at regular intervals [13]. BCNTs have commanded considerable interest recently from the heterogeneous catalysis community as support materials for catalysts used under highly demanding conditions, because their special morphology renders them even more stable mechanically than conventional multiwall carbon nanotubes. Moreover, BCNTs feature high energy defect sites that can be utilized catalytically as well [14].

Catalytic vapor deposition (CVD) is both the most widespread and easiest to use method for nanotube morphology engineering. CVD is a simple and economic technique for synthesizing CNTs compared to arc-discharge and laser-ablation methods, because the CVD method can be carried at much lower temperature and ambient pressure [15]. In a CVD experiment, gaseous carbon sources (most often. hydrocarbons) are thermally decomposed in the presence of catalytically active metals [16, 17]. Carbon sources appropriate for manufacturing bamboo-shaped carbon nanotubes (BCNTs) contain nitrogen (e.g. various amines [18–20]). Different BCNT structures can be obtained by changing the amine type. Modifying the synthesis parameters can significantly affect the yield, the tube diameter and the number of lattice defects. Lattice defects can include vacancies and pentagon-heptagon pairs in the walls of nanotubes [21]. The proper selection of the amine molecule makes it possible to form an active structure that contains high-energy lattice defects.

Raman spectroscopy is an established technique for the characterization of nanotubes [22]. The intensity ratio of the so-called G and D Raman bands depends on the concentration of lattice defects [23–25]. Lattice defects in the outermost nanotube wall play an important role in anchoring functional groups onto the nanotube surface [26]. The dispersibility of nanotubes in solvents can generally be improved by attaching functional groups to them [27]. Moreover, when the carbon nanotubes are used as a catalyst support, the functionalities may also bind metal particles and can even control their size. Chemical surface modification is frequently done by covalent functionalization like the partial oxidation of nanotubes. Besides forming oxygen-containing (–OH, –COOH etc.) functional groups, it is possible to attach other types of functional groups, such as amines, proteins and polymers [28–30] as well.

Different crystal faces of metallic platinum particles behave differently during catalytic and adsorption processes. This is evidenced by the occurrence of different reaction mechanisms in several catalytic reactions, where the sorption of products and reactants changes depending on the crystal plane available on the surface of particles. The adsorption of hydrogen was investigated on defect-free Pt(111) surfaces by Watson et al. [31] and several different adsorption locations were identified with different energy levels. This could explain the three times higher activity in the dehydrocyclization of hexane to benzene over fcc-structured platinum (111) faces compared to Pt(100) surfaces [32]. Other reactions, such as the hydrogenation and dehydrogenation of cyclohexene or other unsaturated hydrocarbons are also frequently investigated to assess the influence of certain crystal faces [33–36]. The catalytic behavior is also affected by particle diameter because the smaller catalyst particle size, the larger the surface area for a given mass of particles. [37].

Carbon nanotubes are often decorated by Pt nanoparticles for catalytic applications. Solhyet and coworkers used Pt/MWCNT in the selective hydrogenation of cinnamaldehyde and it was shown that the best compromise between catalyst activity and selectivity requires low amount of oxygenated groups on the catalysts surface [38]. Li et al. have successfully migrated the electrocatalytic methanol oxidation from its traditional Pt/C catalyst to Pt/MWCNT. The catalyst were prepared by the reduction of a Pt salt in ethylene glycol (EG) solution. By the EG method, the spherical Pt metal particles have high and homogeneous dispersion with narrow particle size distribution [39]. However, results on the synthesis and performance of Pt/BCNT catalysts are not abundant in the literature. Wang et al. utilized Pt/BCNT in methanol oxidation [40] and Shao et al. have compared the electrochemical durability of several Pt-decorated carbon nanotube supports in PEM fuel cells [41].

In this study, we present a facile method of defect engineering in bamboo-shaped carbon nanotubes and explore how defects affect the decoration of the surface with platinum nanoparticles and the hydrogenation activity of the samples. Our results serve as a quick guide in the multivariate parameter space of Pt/BCNT synthesis and create the basis for a more detailed design of experiments study.

Experimental

Materials

Butylamine (Merck Chem.), triethylamine (Merck Chem.) and cyclohexylamine (Scharlau Chem.) were tested as carbon sources for the CNT synthesis (Table S1). Two types of catalysts prepared from iron(III) nitrate nonahydrate ($Fe(NO_3)_3 \cdot 9H_2O$, Reanal) and nickel(II) nitrate hexahydrate ($Ni(NO_3)_2 \cdot 6H_2O$, Merck Chem.) were used. The support for nickel was magnesium oxide (Reanal), while for iron aluminum oxide made from aluminum hydroxide (Reanal) was applied. The dispersing solvent was Patosolv (Molar Chem.), which is a mixture of aliphatic alcohols (ethanol-propanol-butanol).

Synthesis of bamboo shaped carbon nanotubes (BCNTs)

The CCVD synthesis was carried out on two different composition catalysts: 5 % $Fe/Al(OH)_3$ and 5 % Ni/MgO (Table S2). Catalysts were prepared by depositing the transition metal precursors from an aliphatic alcohol mixture (Patosolv) onto the support to obtain a calculated metal loading of 5 wt%. The organic solvent was evaporated in a rotary vacuum evaporator and the product was dried further at 105 °C in a furnace to remove all remnants of the catalysts. The catalyst was reduced in situ by the carbon source stream at the beginning of the CVD synthesis.

The system depicted in Fig. S1 was used in the CVD synthesis. The quartz tube reactor was first inserted by nitrogen, then the amine-containing hydrocarbons were fed into the 150 °C evaporation chamber at a controlled rate by a syringe pump, mixed into the nitrogen carrier stream and introduced into the quartz CVD reactor where the catalyst was placed in a quartz bowl. Nanotubes were synthesized from cyclohexyl amine (CHA), butylamine (BA) and triethylamine (TEA), at atmospheric pressure over different catalysts while all synthesis parameters were kept identical throughout all experiments (T: 750 °C, N_2: 50 mL/min, carbon source 3 mL/h, catalyst loading 0.5 g, synthesis time 20 min).

After the nanotube synthesis, the catalyst was removed by boiling the nanotubes either in a solution of concentrated (36 wt%) hydrochloric acid (iron, magnesia and nickel removal) or in 8 mol/dm^3 sodium hydroxide (alumina dissolution) for 6 h under continuous agitation and reflux [42]. Finally, the CNTs were filtered off, washed with distilled water and dried at 105 °C overnight. The purity of the product was checked by thermogravimetry (TG) and atomic emission spectroscopy (ICP-AES).

Functionalization of BCNTs

Nanotubes were oxidized in a mixture of 65 wt% nitric acid and 98 wt% sulfuric acid (1:3 ratio) for 24 h at room temperature with permanent agitation. The samples were washed using distilled water and then dried at 105 °C overnight.

Decoration of BCNTs with Pt nanoparticles

The synthesized BCNTs were wet impregnated in an aqueous solution of the platinum salt $H_2PtCl_6 \cdot 6H_2O$. 500 mg of BCNTs were dispersed in 200 mL distilled water with ultrasonication for 25 min. The aqueous solution of the platinum complex (66.4 mg of $H_2PtCl_6 \cdot 6H_2O$/50 mL dist. water) were added to the suspension under ultrasonication within 10 min to ensure the precursor was completely dissolved. Water was subsequently removed by a rotary evaporator, then the platinum(IV) salt was decomposed thermally and reduced at 400 °C in hydrogen flow. The platinum content of the samples was approx. 5 wt% as confirmed by ICP measurements.

Characterization

Nanoparticle morphology was studied by Transmission Electron Microscopy (Philips CM 10, 100 kV) and High Resolution Electron Microscopy (FEI Tecnai G2, 200 kV). All samples were drop casted onto 300 mesh copper grids (Ted Pella Inc.) from an aqueous suspension. Quantitative image analysis was done using the ImageJ system. Raman spectra were recorded using a WITEC confocal Raman microscope alpha 300 R equipped with a HeNe-laser emitting light at $\lambda = 632.95$ nm.

Catalytic tests

The catalytic activity of the materials was tested in the hydrogenation of 1-butene in the fixed bed tube reactor depicted in Fig. S2. In each experiment, 100 mg sample was first heated at a rate of 10 °C/min to 450 °C and kept for 1 h in 20 mL/min N_2 flow, then the gas was switched to H_2 (20 mL/min) and the heat treatment was continued for 60 more minutes. The reaction mixture was 20 mL/min H_2 + 20 mL/min N_2 + 10 mL/min 1-butene. The reaction temperature was varied between 0 and 120 °C, and the 1-butene conversion was examined at different temperature.

Infrared spectroscopy was used to monitor the conversion of 1-butene on the basis of the integrated area of the ~ 1646 cm^{-1} peak that corresponds to the $\nu_{C=C}$ vibration. The spectrum of the 20 mL/min H_2 + 20 mL/min N_2 gas mixture was used as reference. The system was individually calibrated at each reaction temperature for five different 1-butene concentrations to ensure a properly linear quantitative response.

Results and discussion

Optimization of the BCNT support synthesis

BCNT synthesis optimization in the multivariate parameter space was carried out by a change one factor at a time strategy and the successive reduction of the number of open variables. The initial parameters of the BCNT synthesis, namely the synthesis

time, temperature, carrier gas flow rate and catalyst loading optimization process were derived from our extensive earlier work on the CVD synthesis of MWCNTs [43–45]. $Al(OH)_3$ and MgO supports were loaded with a total of 5 wt% of transition metals (iron or nickel) and a CVD screening was run using all three amines (BA, TEA, CHA). Catalysts performing below the arbitrary threshold of 15 % amine conversion were not considered any further. This reduced the possible catalyst choices to three: Fe/MgO, Ni/MgO and $Fe/Al(OH)_3$, which were tested in BCNT synthesis while systematically varying the following parameters: amine type, reaction temperature, time. The results are summarized in the Supplementary Information Figs. S3, S4 and S5. The bimetallic system offered the poorest overall performance and was therefore dropped at this point from the optimization. Reaction parameters were fixed as described in "Synthesis of bamboo shaped carbon nanotubes (BCNTs)" section. The obtained carbon yield and amine conversion values are summarized in Table S2.

A characteristic TEM picture presented in Fig. 1a confirms that carbon nanotubes with a bamboo-like structure were synthesized (sample synthesized from butylamine on $Fe/Al(OH)_3$). The quality of the bamboo structural motif as a function of amine type improved in the order TEA < CHA < BA. Varying the reaction temperature between 650 and 800 °C revealed that a higher synthesis temperature shifts the mean tube diameter towards larger values. Similar observations were made earlier by Singh et al. [25]. The arrangement of the graphite planes making up the walls of the tubes can be observed in the corresponding HRTEM image (Fig. 1b). Bamboo shaped nanotubes were obtained on both $Fe/Al(OH)_3$ and Ni/MgO catalysts from all three amine carbon sources. However, significant differences were found in the quality of the BCNT samples. The TEM images in Fig. S6 reveal that the decomposition of CHA on 5 wt% $Fe/Al(OH)_3$ and of TEA on 5 wt% Ni/MgO resulted in samples with broad nanotube diameter distribution, whereas the other four BCNT materials were uniform. Therefore, only the samples BCNT-18, -19, -20 and -22 were considered for further functionalization, Pt decoration and catalytic testing.

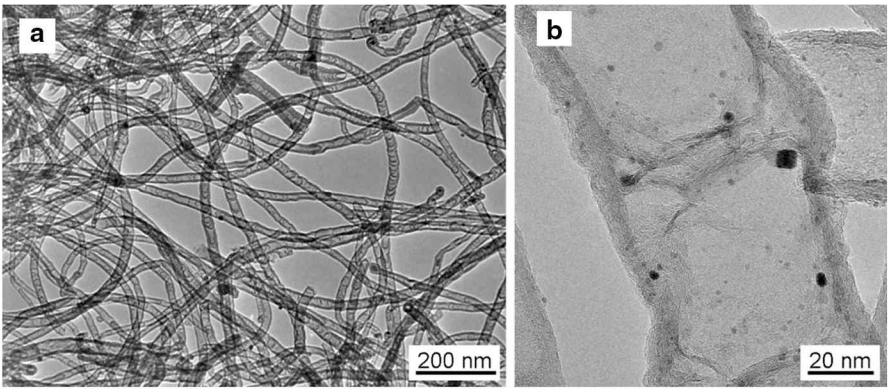

Fig. 1 TEM (**a**) and HRTEM (**b**) image of BCNTs synthesized from butylamine on $Fe/Al(OH)_3$

A Raman spectroscopic study was undertaken to determine the concentration of lattice defects as a function of synthesis parameters. Spectra are presented in Fig. 2a and a typical HRTEM image exemplifies nanotube structural distortion, lattice defects and carbonaceous debris in Fig. 2b. The Raman peak found at 1390 cm^{-1} is the so-called D band or 'defect vibration' caused by phonon scattering on sp^3 carbon atoms and the one at 1590 cm^{-1} is the G band which can be attributed to the in-plane stretching vibrations of the perfect sp^2 graphitic structure [22]. Therefore, the structural integrity of carbon nanotubes can be characterized by comparing the intensity ratio of these two peaks (I_D/I_G, see Fig. 2a). Samples BCNT 19 and BCNT 20 (both synthesized over Ni) exhibit the largest relative defect concentration (highest I_D/I_G ratio) and BCNT 22 is the most defect-free structure.

BCNT functionalization and Pt decoration

The surface of the bamboo-shaped carbon nanotubes was functionalized by oxidation in acidic media to facilitate the attachment of noble metal nanoparticles to the BNCTs. Oxidative treatment was found to reduce the length of the nanotubes from several microns to 100-200 nm long sections as depicted in Fig. 3a. The corresponding increase in nanotube fissure induced defect concentration is indicated by the increased I_D/I_G ratio (Fig. 3b; Table 1). It is interesting to note that sample BCNT-22 suffered the largest increase in defect site density during functionalization.

Functionalization has increased the hydrophilic character of the carbon nanotubes, which may render them more soluble in aqueous media. This effect was quantified by preparing aqueous BCNT suspensions and measuring the electrokinetic potential of the functionalized nanotubes in aqueous medium. Electrophoretic measurements were performed with an NZ Zeta NanoSizer instrument (Malvern). The values obtained for electrophoretic mobility were converted into zeta-potentials using the classical Smoluchowski formula. This approach disregards the so-called breaking effect of induced dipole moments on

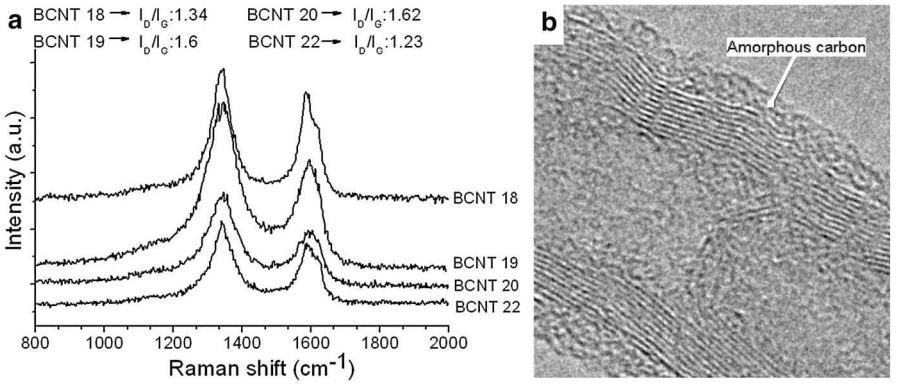

Fig. 2 **a** Raman spectra of the BCNTs and data for I_D/I_G all samples, **b** HRTEM image of the BCNT 18

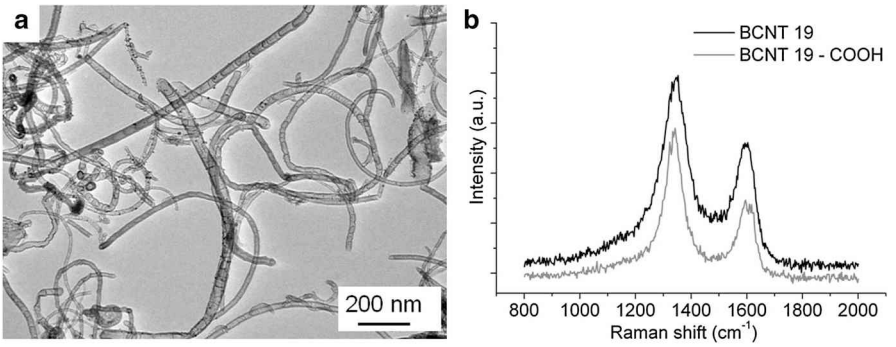

Fig. 3 **a** TEM image of the BCNT oxidized with mixtures of H_2SO_4/HNO_3, **b** Raman spectra of the non-functionalized and functionalized nanotubes

Table 1 I_D/I_G ratios of the treated and non-treated nanotubes as well as values of the peak areas defined based upon the FTIR spectra and the electrokinetic potential values

	BCNT 18	BCNT 19	BCNT 20	BCNT 22
Raman I_D/I_G				
Untreated BCNT	1.34	1.60	1.62	1.23
BCNT-COOH	1.67	1.68	1.66	1.80
Zeta potential (mV)	−42.1 ± 6.3	−20.6 ± 2.9	−54.4 ± 6.6	−46.9 ± 4.2

electrophoresis—potentially a rising from the EDL polarization of thick double layers (i.e. at low ionic strength). Therefore, the values given below virtually represent the "efficient" ζ-potentials of the nanotubes, calculated as electrophoretic mobility multiplied by the ratio of viscosity to permittivity (of the medium). As obvious from the literature, this calculation method is worldwide accepted, for purposes of easy data comparison, e.g. it allows researchers to follow the effect of different variables on the electrophoretic mobility and zeta-potentials of CNTs [46]. Data summarized in Table 1 indicate that the formation of –COOH groups on the BCNT surface invariable resulted in a negative zeta potential. The zeta potential was below −30 mV for three out of the studied four BCNT suspensions, which remained stable for 24 h. Sample BCNT 19 was functionalized to a less extent according to FTIR measurement of the –COOH band intensity (not shown). Its zeta potential was only −20 mV, therefore, it aggregated in the aqueous suspension after 10 min (Fig. S7).

Functional groups could serve as anchor points for platinum nanoparticles on the BCNT surface [41]. These could be prepared in situ by wet impregnation and subsequent reduction on the nanotube surface. TEM image analysis revealed that the size distribution of the formed Pt nanoparticles was governed by the functional group concentration (Table 2).

Table 2 Characterization of platinum decorated bamboo shaped carbon nanotube catalysts

	S_{BET} (m^2/g)	Pt content (m/m %)	d_{Pt} (nm)	Pt dispersion
Pt/BCNT-18	90.7	5.13	6.7	0.24
Pt/BCNT-19	140.4	5.07	3.8	0.42
Pt/BCNT-20	146.1	5.02	3.9	0.41
Pt/BCNT-22	124.9	5.01	5.0	0.32

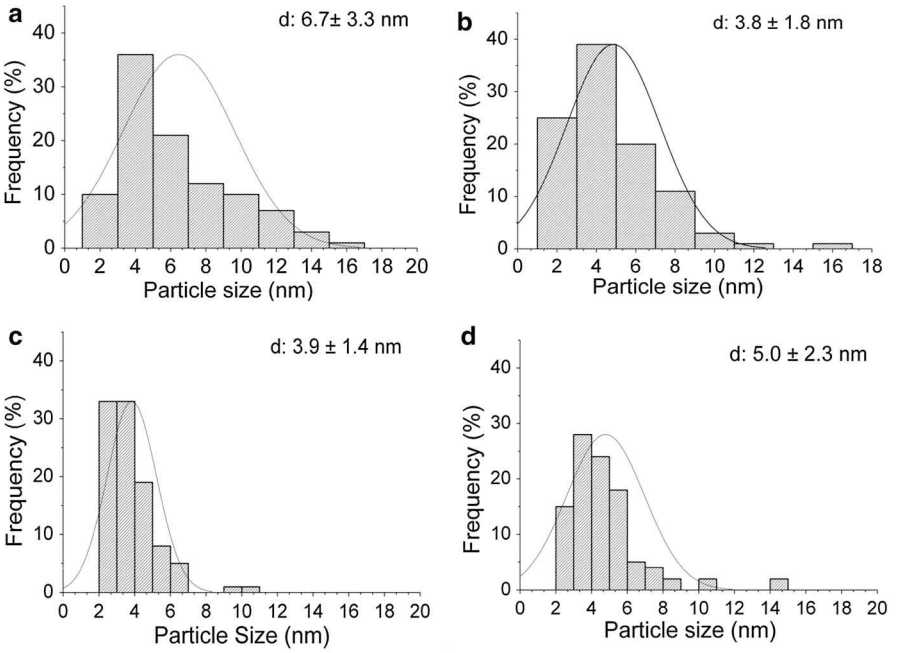

Fig. 4 Diameter distribution of Pt nanoparticles in Pt/BCNT catalyst samples: **a** BCNT 18, **b** BCNT 19, **c** BCNT 20 and **d** BCNT 22

Platinum dispersion values (D. %/100) were calculated according to Freund et al. [47] using Eq. 1:

$$D = \frac{6A}{\rho \delta L d} \tag{1}$$

Here A is the atomic mass of platinum (195.08 g/mol), ρ is the density of bulk platinum (21.45 g/cm^3), δ is average surface area occupied by one Pt atom (5.72×10^{-20} m^2), L is Avogadro's constant and d is the average Pt nanoparticle diameter from TEM. Pt particles grew larger on samples with more carboxyl groups (BCNT 18 and 22) and smaller on surfaces functionalized to a lesser extent (BCNT 19 and 20). This phenomenon can be explained by considering the platinum balance between the surface and the aqueous solution: more anchor points concentrate

platinum on the BCNT surface, while if the concentration of anchors is low then nanoparticle growth becomes primarily a solution-based process. These results indicate that by controlling the surface functionality of bamboo-shaped carbon nanotubes it is possible to tailor their platinum nanoparticle decoration according to user requirements (Fig. 4).

1-butene hydrogenation activity of Pt/BCNT catalysts

A typical temperature series of IR spectra obtained on the Pt/BCNT-20 sample is presented in Fig. 5. The integrated area of the $\nu_{C=C}$ peak at 1646 cm^{-1} was used to calculate the 1-butene contents of the system.

Additional verification about the reaction progress and the lack of side reactions was provided by the decreasing peaks corresponding to vibrations $\nu_{as.(=CH2)}$ between 3075 and 3095 cm^{-1} and $\gamma_{(=CH2)}$ at $\sim$916 cm^{-1}. All four BCNT supports were tested without Pt nanoparticles at all reaction temperatures considered, and found to be inactive in 1-butene hydrogenation.

The conversion values of 1-butene were calculated by Eq. 2:

$$X\,\% = \frac{n_{butene}^{reacted}}{n_{butene}^{fed}} \times 100 \tag{2}$$

The initial phase of the test reactions is depicted in Fig. 6. All catalysts require an initiation period of 5–8 min. Those featuring BCNT supports synthesized from butylamine (Figs. 5b and 6a) were only active above 100 °C reaction temperature, whereas the other two samples exhibited appreciable 1-butene conversions even below room temperature (Fig. 5d and 6c) and increasing the reaction temperature any further had only a minor effect on their performance. Similar maximal 1-butene conversion in the 80–98 % range were achieved on all samples, with Pt/BCNT-22 (Fig. 6d) being the most active of the four.

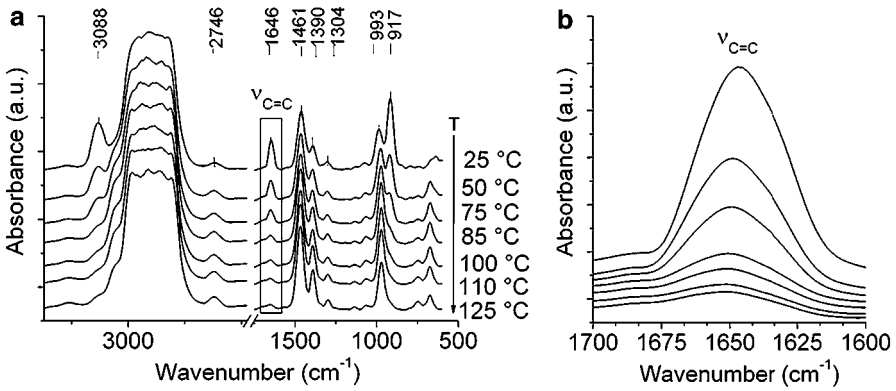

Fig. 5 **a** Temperature series of infrared spectra recorded after 10 min of reaction time over Pt/BCNTs-22 catalyst, **b** a detailed view of the evolution of the $\nu_{C=C}$ band used for quantitative catalyst performance assessment

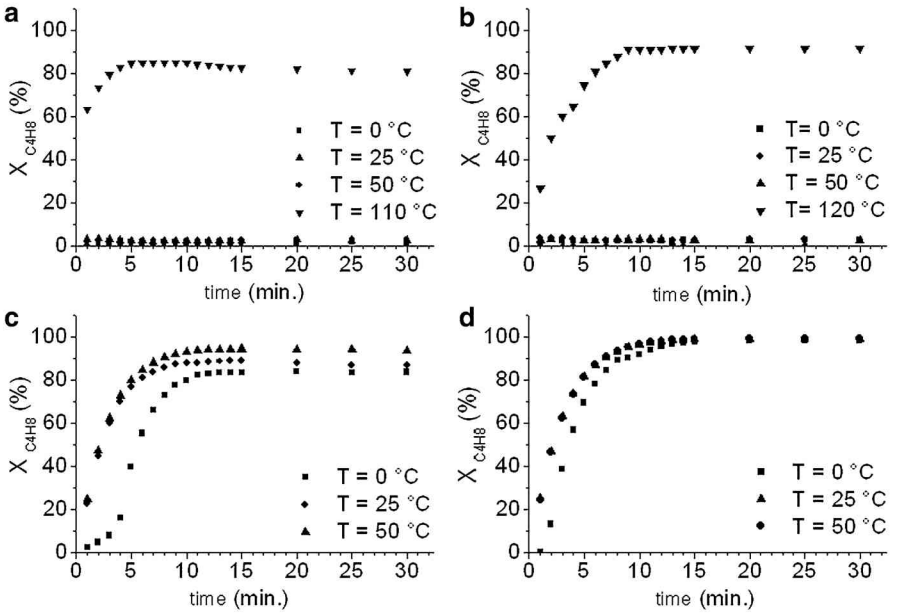

Fig. 6 Initiation of the tested catalysts in the 1-butene hydrogenation reaction. Pt/BCNT-18 (**a**). Pt/BCNT-19 (**b**). Pt/BCNT-20 (**c**) and Pt/BCNT-22 (**d**)

The plateau-like appearance of the 1-butene conversion versus time functions suggests that the catalyst performance can be maintained for long periods of time. Time-on-stream tests run for 4 h were performed to verify this hypothesis. Data presented in Fig. 7. suggest that some catalyst deactivation occurred in the case of Pt/BCNT-18 sample, while the other three samples have not suffered any activity losses over the studied period.

The best overall performance was achieved on the Pt/BCNT-22 sample. It is interesting to note that neither the specific surface area nor the Pt dispersion of this material were the highest among the studied materials, however, its defect site density was the lowest before functionalization and the highest after functionalization as determined from the Raman I_D/I_G ratio. This finding confirms that the defect engineering of bamboo shaped carbon nanotube supports is critically important when tuning the performance of novel catalysts.

Conclusion

The CVD synthesis of bamboo-shaped carbon nanotubes from amine precursors over iron (Fe) and nickel (Ni) containing supported catalysts (5 % $Fe/Al(OH)_3$ and 5 % Ni/MgO) was optimized by the successive reduction of the dimensionality of an initially very large parameter space. The choice of CVD catalyst has severely affected the carbon yield and the quality of the obtained BCNTs. The surface of the BCNTs was oxidatively functionalized and the formed –COOH groups were used to

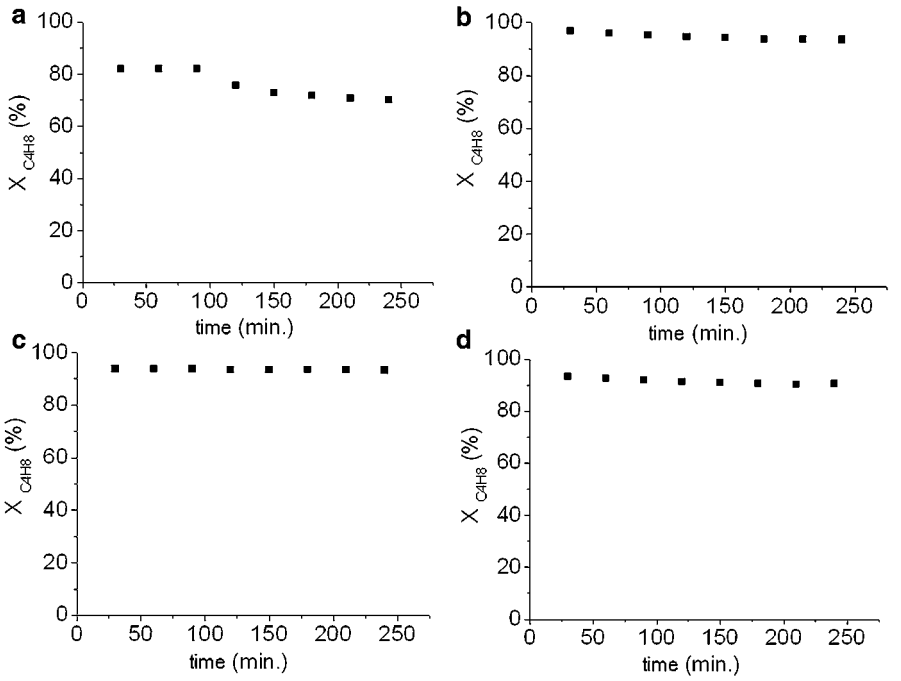

Fig. 7 1-Butene conversion as a function of time over Pt/BCNT-18 at 120 °C (**a**), Pt/BCNT-19 at 120 °C (**b**), Pt/BCNT-20 at 50 °C (**c**) and Pt/BCNT-22 at °C (**d**)

anchor sub-10 nm platinum nanoparticles to the surface. The diameter of Pt nanoparticles formed in situ could be tailored by controlling the defect site density of the nanotubes. The performance of four optimized Pt/BCNT catalysts was tested in the hydrogenation of 1-butene. The best overall performance was achieved on the Pt/BCNT-22 sample (BCNTs synthesized on 5 wt% $Fe/Al(OH)_3$ from triethylamine) where a butene conversion above 98 % was combined with rapid initiation (85 % of the maximum butene conversion reached within 5 min after starting the reaction at 25 °C) and long-term catalyst stability. Our findings confirm that defect engineering of the support is critical for developing new carbon nanomaterial supported hydrogenation catalysts and pave the way for a more detailed multivariate optimization of novel bamboo shaped carbon nanotube supports.

Acknowledgments This research was partially carried out in the framework of the Center of Applied Materials Science and Nano-Technology at the University of Miskolc. The financial support of the OTKA NN 110676 and OTKA K 112531 Projects is acknowledged.

References

1. Yu Z, Fareid LE, Moljord K, Blekkan EA, Walmsley JC, Chen D (2008) Appl Catal B 84:482–489
2. Zhang Y, Zhang HB, Lin GD, Chen P, Yuan YZ, Tsai KR (1999) Appl Catal A 187:213–224
3. Bahome MC, Jewell LL, Hildebrandt D, Glasser D, Coville NJ (2005) Appl Catal A 287:60–67
4. Ovejero G, Sotelo JL, Rodriguez A, Diaz C, Sanz R, Garcia J (2007) Ind Eng Chem Res 46:6449–6455

5. Chen WY, Ji J, Feng X, Duan XZ, Qian G, Li P, Zhou XG, Chen D, Yuan WK (2014) J Am Chem Soc 136:16736–16739
6. Chambers A, Nemes T, Rodriguez NM, Baker RTK (1998) J Phys Chem B 102:2251–2258
7. Serp P, Corrias M, Kalck P (2003) Appl Catal A253:337–358
8. Pham-Huu C, Kelle N, Ehre G, Charbonniere LJ, Ziessel R, Ledoux MJ (2001) J Mol Catal A 170:155–163
9. Onoe T, Iwamoto S, Inoue M (2007) Catal Commun 8:701–706
10. Liao HG, Xiao YJ, Zhang HK, Liu PL, You KY, Luo H, Wei C (2012) Catal Commun 19:80–84
11. Pereira MFR, Figueiredo JL, Oerfaó JJM, Serp P, Kalck P, Kihn Y (2004) Carbon 42:2807–2813
12. Liu X, Su DS, Schlogl R (2008) Carbon 46:544–561
13. Liu H, Zhang Y, Li R, Sun X, Desilets S, Abou-Rachid H, Jaidann M, Lussier LS (2010) Carbon 48:1498–1507
14. Gan L, Lv L, Du H, Li B, Kang F (2009) Carbon 47:1833–1840
15. Kumar M, Ando Y (2010) J Nanosci Nanotechnol 10:3739–3758
16. Joseyacaman M, Mikiyoshida M, Rendon L, Santiesteban JG (1993) Appl Phys Lett 62:657–659
17. Endo M, Takeuchi K, Kobori K, Takahashi K, Kroto HW, Sarkar A (1995) Carbon 33:873–881
18. KovalevskiV SafronovAN (1998) Carbon 36:963–968
19. Mayne M, Grobert N, Terrones M, Kamalakaran R, Rühle M, Kroto HW, Walton DRM (2001) Chem Phys Lett 338:101–107
20. Reyes M, Grobert N, Kamalakaran R, Seeger T, Golberg D, Rühle M, Bando Y, Terrones H (2004) Chem Phys Lett 396:167–173
21. Collins PG (2009) In: Narlikar AV, Fu YY (eds) Defects and disorder in carbon nanotubes in Oxford handbook of nanoscience and technology: frontiers and advances. Oxford University Press, Oxford
22. Dresselhaus MS, Dresselhaus G, Saito G, Jorio A (2005) Phys Rep 409:47–99
23. Hussain S, Jha P, Chouksey A, Raman R, Islam SS, Islam T, Choudhary PK (2011) J Mod Phys 2:538–543
24. Skákalová V, Kaiser AB, Dettlaff-Weglikowska U, Hrncariková K, Roth S (2005) J Phys Chem B 109:7174–7181
25. Singh C, Shaffer MSP, Windle AH (2003) Carbon 41:359–368
26. Reddy ALM, Ramaprabhu SR (2007) Int J Hydrog Energy 32:3998–4004
27. Osorio AG, Silveira ICL, Bueno VL, Bergmann CP (2008) Appl Surf Sci 30:2485–2489
28. Men XH, Zhang ZZ, Song HJ, Wang K, Jiang W (2008) Compos Sci Technol 68:1042–1049
29. Shen J, Huang W, Wu L, Hu Y, Ye M (2007) Mat Sci Eng A 46:151–156
30. Kitano H, Tachimoto K, Anraku Y (2007) J Colloid Interface Sci 306:28–33
31. Fearon J, Watson GW (2006) J Mater Chem 16:1989–1996
32. Davis SM, Zaera F, Somorjai GA (1984) J Catal 85:206–223
33. Campbell CT, Sun YK, Weinberg WH (1991) Chem Phys Lett 179:53–57
34. McCrea KR, Somorjai GA (2000) J Mol Catal A 16:43–53
35. Bratlie KM, Flores LD, Somorjai GA (2005) Surf Sci 599:93–106
36. Bratlie KM, Somorjai GA (2007) J Phys Chem C 111:6837–6845
37. Valden M, Lai X, Goodman DW (1998) Science 281:1647–1650
38. Solhy A, Machado BF, Beausolei J, Kihn Y, Gonçalves F, Pereira MFR, Órfão JJM, Figueiredo JL, Faria JL, Serp P (2008) Carbon 46:1194–1207
39. Li W, Liang C, Zhou W, Qiu J, Zhou Z, Sun G, Xin Q (2003) J Phys Chem B 107:6292–6299
40. Wang CH, Du HY, Hsu HC, Chang ST, Huang HC, Chen LC, Chen KH (2012) Int J Hydrog Energy 37:10663–10670
41. Shao Y, Kou R, Wang J, Wang CM, Vishwanathan VV, Liu J, Wang Y, Lin Y (2009) J Nanosci Nanotechnol 9:5811–5815
42. Pillai SK, Ray SS, Moodley M (2008) J Nanosci Nanotechnol 8:6187–6207
43. Kukovecz A, Konya Z, Nagaraju N, Willems I, Tamasi A, Fonseca A, Nagy JB, Kiricsi I (2000) Phys Chem Chem Phys 2:3071–3076
44. Szabó A, Méhn D, Kónya Z, Fonseca A, Nagy JB (2003) Phys Chem Comm 6:40–41
45. Nagy JB, Bister G, Fonseca A, Méhn D, Kónya Z, Kiricsi I, Horváth ZE, Biró LP (2004) J Nanosci Nanotechnol 4:326–345
46. Vanyorek L, Meszaros R, Barany S (2014) Colloids Surf A 448:140–146
47. Lear T, Marshall R, Sanchez AL, Jackson D, Klapötke TM, Bäumer M, Rupprechter G, Freund H, Lennon D (2005) J Chem Phys 123:174706